Fuel 387 (2025) 134419

Contents lists available at ScienceDirect

Fuel

journal homepage: www.elsevier.com/locate/fuel

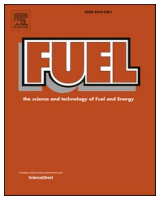

Full Length Article

# Enhancing biomass chemical looping gasification for hydrogen production: Synergistic effect of in-situ $NaAlO_2$ on $Fe_2O_3$/EAFS

Laixing Luo [a,1], Zhihang Lai [b,c,1], Xing Zheng [a], Zongming Zheng [a], Xianbin Xiao [a,e], Wu Qin [a,d,*]

[a] School of New Energy, North China Electric Power University, Beijing 102206, China
[b] Guangzhou Institute of Energy Conversion, Chinese Academy of Sciences, Guangzhou 510640, China
[c] School of Energy Science and Engineering, University of Science and Technology of China, Hefei 230026, China
[d] School of Engineering, China University of Petroleum-Beijing at Karamay, Xinjiang 834000, China
[e] Shanxi Research Institute of Huairou Laboratory, Taiyuan 030032, China

ARTICLE INFO

*Keywords:*
Chemical looping gasification
Biomass
Hydrogen
Oxygen carrier
$NaAlO_2$

ABSTRACT

Although electric arc furnace slag (EAFS) is widely acknowledged for its rich oxide composition, encompassing $SiO_2$, CaO, and $Al_2O_3$, as well as its advantageous effects at polycrystalline grain boundaries, its broader industrial utilization remains constrained by challenges associated with surface hardness and high-temperature passivation. In this investigation, we adopted an innovative methodology that integrates physical grinding and chemical surface modification to in situ transform $Al_2O_3$ into $NaAlO_2$ within EAFS. $NaAlO_2$, distinguished by its elevated melting point and catalytic activity, emerges as a superior alternative to the conventional biomass gasification catalyst, $Na_2CO_3$, as it effectively mitigates issues such as slagging, fouling, corrosion, and alkali metal volatilization. Moreover, $NaAlO_2$ facilitates the cleavage of macromolecular bonds in biomass during the early stages of gasification, thereby promoting the generation of small-molecule gases, and serves as a catalyst in the reduction reaction between $Fe_2O_3$/EAFS and gaseous organic molecules. Utilizing $NaAlO_2$-$Fe_2O_3$/EAFS as the oxygen carrier, our experiments demonstrated an optimal hydrogen generation rate of 0.559 L per 0.5 g of material at 750 °C, with an excess oxygen ratio (Ω) of 0.2. Thermodynamic and kinetic analyses further corroborated the synergistic effect of $NaAlO_2$ on $Fe_2O_3$/EAFS, enhancing both carbon conversion and hydrogen production. In situ converting $Al_2O_3$ into $NaAlO_2$ and supporting $Fe_2O_3$ on EAFS as a dual-functional material not only improved the energy conversion efficiency of biomass gasification but also presented a viable strategy for addressing solid waste management challenges.

## 1. Introduction

Chemical Looping Combustion (CLC) [1], an advanced combustion technology, attracts widespread attention. The revolutionary concept behind this technology involves moving away from the direct contact between oxygen and fuel in traditional air combustion processes, instead utilizing metal or non-metal oxygen carriers (OCs) as intermediates for the oxidation reaction. In the CLC system, OC first react with oxygen to acquire oxygen atoms, which are then transferred to the fuel for combustion, thereby preventing the formation of harmful $NO_x$ pollutants through the combination of nitrogen and oxygen at high temperatures. Moreover, the separation of $CO_2$ from the unreacted OC after combustion provides unprecedented convenience for the efficient capture and storage of $CO_2$ [2], making CLC a prominent candidate technology for future low-carbon energy conversion. This principle is also applicable to Chemical Looping Gasification (CLG), which involves a two-step reaction process: fuel reacts with OC in a nitrogen-free atmosphere to produce syngas (mainly consisting of $H_2$ and CO), followed by a oxidation step to recover the OC for recycling [3–5]. Fan et al. have further explored the application of CLG for large-scale hydrogen production [6], highlighting its advantages over traditional gasification methods, including lower costs, effective utilization of OC as a heat source, high purity of produced syngas, reduced tar formation, and significantly lower emissions of pollutants during the gasification

* Corresponding author at: School of New Energy, North China Electric Power University, Beijing 102206, China.
*E-mail address:* qinwu@ncepu.edu.cn (W. Qin).
[1] Laixing Luo and Zhihang Lai contributes equally to this work.

https://doi.org/10.1016/j.fuel.2025.134419
Received 15 October 2024; Received in revised form 26 December 2024; Accepted 15 January 2025
Available online 21 January 2025

process [7–13].

Currently, OCs used in CLG primarily consist of transition metal oxides such as Ni, Cu, Fe, and Mn. Fe-based OCs are particularly prevalent in CLG applications for processing organic solid waste, especially in the "steam-iron cycle" process [14–16]. Their widespread use is attributed to their low cost, environmental sustainability, high mechanical strength, and exceptional resistance to sintering, making them a focus of extensive research [17–21]. To enhance the stability and reactivity of Fe-based OCs, researchers have explored the incorporation of inert supports to improve both their physical and chemical properties. Inert supports, such as $Al_2O_3$, provide robust structural reinforcement while also being economical, non-toxic, and safe. Inert supports improve the mechanical durability of OCs, increase porosity and specific surface area, and effectively mitigate sintering during extended operation, thereby prolonging the lifespan of the OCs [22–24]. Modifying the inert support not only enhances lattice oxygen transfer properties but also improves the mechanical characteristics of OCs. By optimizing the impregnation process and constructing an $MgO/TiO_2$ inert support, research has shown that this approach can enhance sintering resistance and crushing strength of OCs during cycling [25]. In a separate study, $Fe_2O_3/ZrO_2$ was combined with organic compounds, followed by the removal of these organics at high temperatures to form a porous $ZrO_2$ shell. The resulting OCs exhibited a stable pore structure, specific surface area, and core–shell morphology, demonstrating excellent redox activity and sintering resistance [26].

Electric arc furnace slag (EAFS), a by-product of industrial smelting, is commonly recycled as a flux in blast furnace smelting, reintegrated into steelmaking processes, utilized in hot metal pretreatment, and repurposed for the production of construction materials, fertilizers, and soil amendments [27–32]. Despite the maturity of existing slag recycling technologies, the overall utilization rate of EAFS remains suboptimal, with certain valuable elements in the slag not fully recovered or leveraged for high-value-added applications [33–46]. EAFS is rich in CaO, MgO, MnO, and $Al_2O_3$, along with significant amounts of FeO and Fe. These characteristics make EAFS a suitable material as an OC for CLG processes. Studies have confirmed the feasibility of using steel converter slag as an OC in CLG processes [47,48]. It has been found that EAFS exhibits a higher carbon conversion rate and stable reactivity compared to other types of slag [49]. One study assessed EAFS as an OC in fuel CLC processes under 800 °C fluidized bed conditions over 50 cycles, achieving a fuel gas conversion rate exceeding 85 % [50,51]. Another investigation demonstrated that transforming calcium-containing components in steel slag into $CaSO_4$ through a pre-sulfating step can achieve almost complete CO conversion at temperatures below 800 °C during the CLC process [52]. The reactivity of OCs can be enhanced through both alkali impregnation and acid impregnation. Alkali impregnation facilitates the formation of an intermediate C-O-M structure within OC, which alters the electron cloud density on the coke surface, weakens C–C bonds, promotes the adsorption of $CO_2$ and $H_2O$ molecules, and accelerates the gasification reaction [53,54]. Acid impregnation increases the surface area and porosity of oxygen carriers, thereby enhancing their reactivity. Furthermore, it has been observed that acid modification significantly improves the generation rate and selectivity of $C_2$ oxygen-containing compounds on certain catalyst supports [55].

Given the analogous metal oxide compositions in industrial waste slags and the requisite characteristics for CLG OCs, along with the polycrystalline grain boundaries in slags that offer additional active sites, this study presents a novel approach by entailing the physical modification and chemical activation of industrial waste slags to convert them into high-performance OCs for low-grade fuel CLG hydrogen production. Specifically, in situ conversion of $Al_2O_3$ in EAFS to $NaAlO_2$ through chemical activation enhances the early stages of biomass gasification by promoting bond cleavage and small molecular gas formation. Additionally, the high melting point of $NaAlO_2$ effectively mitigates common operational issues such as slagging, fouling, corrosion, and alkali metal volatilization. This transformation not only optimizes the utilization of waste slag resources but also markedly improves hydrogen production efficiency and the overall performance of the CLG system. Such advancements contribute significantly to the development of sustainable and eco-friendly energy technologies on both a national and global scale.

## 2. Methods

### 2.1. Materials

In the CLG process, corn stalk is employed as the biomass feedstock, while $Fe_2O_3$ serves as the OC, supported on EAFS, blast furnace slag (BFS), and $Al_2O_3$. These materials are designated as $Fe_2O_3$/EAFS, $Fe_2O_3$/BFS, and $Fe_2O_3/Al_2O_3$, respectively. The raw EAFS and BFS were sourced from Fujian Sanbao Steel Co., Ltd. The proximate analysis and ultimate analysis of the corn stalk were shown in Table 1. The elemental compositions and concentrations of EAFS and BFS are provided in Table 2.

To enhance loading efficiency and improve reaction activity, the slag underwent a series of surface activation modifications, including alkali impregnation, acid impregnation, and mechanical milling. During the alkali impregnation step, the carrier particles were treated with a 1 mol/L NaOH solution for 3 h to facilitate effective leaching and chemical conversion. Subsequently, the modified material was dried and solidified at a constant temperature of 80 °C for 8 h, ensuring thorough dehydration and stabilization of the introduced chemical functionalities.

During the acid impregnation phase, 1 mol/L acetic acid (HAC) solution was utilized as the modifying medium. The carrier particles were immersed for 3 h to facilitate the extraction or alteration of chemical components, promoting modifications in surface structure. Following the acid treatment, the same drying protocol was applied, where the material was dried at 80 °C for 8 h to achieve the desired physical state.

In the subsequent mechanical milling process, the impregnated slag carrier particles were uniformly mixed with deionized water and subjected to fine milling for several hours to reduce particle size, increase specific surface area, and enhance surface roughness. After milling, solid–liquid separation was performed through filtration, and the solid phase was dried at a constant temperature of 80 °C for 8 h, yielding fully activated and modified slag carrier materials with improved performance.

Three iron-based OCs ($Fe_2O_3$/EAFS, $Fe_2O_3$/BFS, and $Fe_2O_3/Al_2O_3$) were prepared via the impregnation method [56], with the active $Fe_2O_3$ content maintained at 60 wt%. In this process, EAFS (or BFS and $Al_2O_3$) was first thoroughly mixed with a saturated aqueous solution of Fe $(NO_3)_3$ under continuous stirring. The mixture was then dried at 100 °C for 8 h. In cases where $Al_2O_3$ served as the carrier, the dried product was further ground into a fine powder with a particle size between 60 and 80 mesh. These powders were subsequently employed in biomass CLG-related experimental studies.

### 2.2. Performance and analysis

Fig. 1 presents a detailed schematic of the experimental workflow for

**Table 1**
Proximate analysis and ultimate analysis of the corn stalk.

| As received (ar) | | |
|---|---|---|
| Proximate analysis (wt%) | Volatile (Var) | 67.42 |
| | Fixed carbon (Far) | 12.94 |
| | Ash (Aar) | 9.35 |
| | Moisture (Mar) | 10.29 |
| Ultimate analysis (wt%) | Carbon (Car) | 41.14 |
| | Hydrogen (Har) | 5.94 |
| | Nitrogen (Nar) | 0.58 |
| | Oxygen (Oar) | 32.54 |
| | Sulfur (Sar) | 0.17 |

**Table 2**
The chemical components of raw EAFS, BFS and WSCR.

| Slag's chemical components | O | Fe | Ca | Si | Mn | Mg | Al | Ti |
|---|---|---|---|---|---|---|---|---|
| EAFS | 33.850 | 26.435 | 19.675 | 6.176 | 5.267 | 4.520 | 1.858 | 0.408 |
| BFS | 41.108 | 0.480 | 27.711 | 15.597 | 0.405 | 3.713 | 8.766 | 0.606 |

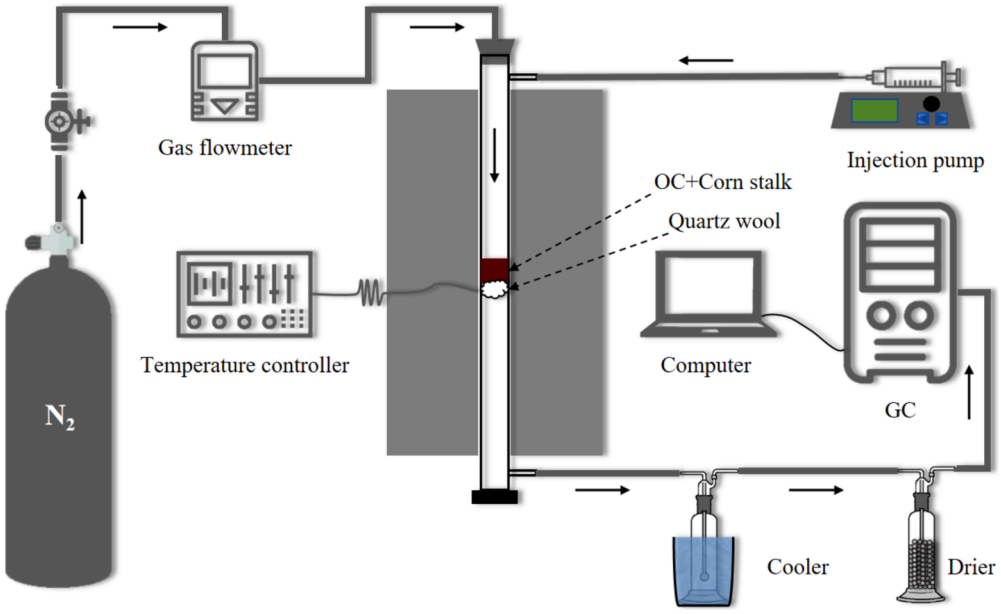


**Fig. 1.** The biomass CLG experimental system.

biomass CLG. The experimental setup comprises an injection pump, a tubular furnace, a gas introduction system, a quartz reaction tube with an inner diameter of 18 mm and a length of 900 mm, a drying apparatus, a cooler, and an Agilent 490 Micro GC gas chromatograph [56]. For each experiment, a mixture of 0.5 g of corn stalk powder and the $Fe_2O_3$/ carrier composite is loaded into the quartz reaction tube, which is then accurately positioned within the electric furnace. The procedure begins by purging the reaction chamber with nitrogen gas at a flow rate of 160 mL/min, ensuring a nitrogen concentration exceeding 99 % by volume. After completing the nitrogen flush, the furnace is activated to heat the system to the target temperature. At this stage, deionized water is injected at a rate of 0.333 mL/min using the injection pump. Simultaneously, nitrogen flow resumes at 160 mL/min, while the gas chromatograph, positioned inline, continuously analyzes the gaseous emissions from the reaction system in real time.

In order to alleviate the problems of scaling and corrosion caused by the volatility of alkali, deactivation of alkali catalysts, and slagging of low melting point alkali containing substances during catalytic gasification, catalytic gasification is usually carried out within the temperature range of 600–900 ℃ [57]. Previous studies have demonstrated that hydrogen production in catalytic gasification reaches its peak when Ωis approximately 0.2 [56]. However, as Ω increases beyond this optimal point, the intensity of oxidation reactions within the reactor also increases. This leads to a decline in hydrogen production efficiency due to excessive oxidation.

### 2.3. Data evaluation

Data evaluation followed the same methodology as outlined in our previous work [56]. Utilizing the conservation of nitrogen, the gas output flow rate at any given time ($t$), denoted as $Qt$, was calculated using the following approach:

$$Q_t = \frac{Q_{N_2}}{1 - x_{H_2} - x_{CO} - x_{CH_4} - x_{CO_2}} \quad (1)$$

where $Q_{N_2}$ is the inlet $N_2$ flow rate set at 160 mL/min, $x_{H_2}$, $x_{CO}$, $x_{CH_4}$ and $x_{CO_2}$ are the volume fraction of the outlet gas $H_2$, CO, $CH_4$, and $CO_2$ at reaction time (t) measured by the gas chromatograph, respectively. The flow rate for each outlet gas at reaction time (t) could be calculated as follows:

$$Q_{H_2}(t) = Q_t \times x_{H_2} \quad (2)$$

$$Q_{CO}(t) = Q_t \times x_{CO} \quad (3)$$

$$Q_{CH_4}(t) = Q_t \times x_{CH_4} \quad (4)$$

$$Q_{CO_2}(t) = Q_t \times x_{CO_2} \quad (5)$$

Then the total volume of the generated gas was calculated as follows:

$$V_{H_2} = \int Q_{H_2}(t)dt \quad (6)$$

$$V_{CO} = \int Q_{CO}(t)dt \quad (7)$$

$$V_{CH_4} = \int Q_{CH_4}(t)dt \quad (8)$$

$$V_{CO_2} = \int Q_{CO_2}(t)dt \quad (9)$$

Oxygen excess ratio ($\Omega$) was calculated as follows:

$$n_{O_2} = 0.5 \times \left(\frac{C_{ar}}{12} + \frac{H_{ar}}{4} + \frac{S_{ar}}{32} - \frac{O_{ar}}{32}\right) \quad (10)$$

$$\Omega = \frac{0.4 \times m_{OC}}{160 \times n_{O_2}} \quad (11)$$

where $C_{ar}$, $H_{ar}$, $S_{ar}$ and $O_{ar}$ are the as received basis of carbon, hydrogen, sulfur, and oxygen in the corn stalks. $m_{OC}$ is the mass of the OC.

## 3. Results and discussion

### 3.1. Effect of different slags

In the biomass CLG process, the OC serves a dual role as both an oxidant, facilitating partial oxidation of the fuel, and as a catalyst, enhancing carbon conversion and gasification reactions [11–17]. A comparative analysis of corn stalk CLG was conducted using $Fe_2O_3$/EAFS, $Fe_2O_3$/BFS, $Fe_2O_3$/WSCR, and $Fe_2O_3/Al_2O_3$ as OCs at a temperature of 800 °C and $\Omega$ of 0.2. The performance results are illustrated in Fig. 2. $Fe_2O_3$/BFS exhibited the lowest hydrogen production rate, with a maximum flow rate of 6.2 mL/min. Conversely, $Fe_2O_3/Al_2O_3$ and $Fe_2O_3$/EAFS achieved significantly higher maximum hydrogen flow rates of 21.6 mL/min and 26.8 mL/min, respectively. The cumulative hydrogen yields for $Fe_2O_3/Al_2O_3$ and $Fe_2O_3$/EAFS were comparable. Notably, even in the absence of surface modification, EAFS loaded with $Fe_2O_3$ demonstrated superior catalytic activity compared to BFS. This enhanced performance is likely due to the higher iron content and lower silicon content in EAFS (Table 1). The elevated $SiO_2$ concentration in BFS can lead to the formation of inert $Fe_2SiO_4$ under high-temperature conditions, which impedes the catalytic partial oxidation of corn stalks [58]. Additionally, while the $Al_2O_3$ content in untreated EAFS is lower than that in BFS, its multi-component composition and boundary effects confer catalytic properties similar to $Al_2O_3$. For instance, the high Mg/Al ratio in EAFS has been shown to regulate the $Fe^{2+}/Fe^{3+}$ ratio, thereby promoting lattice oxygen migration in $Fe_2O_3$ and enhancing its reactivity [59]. Furthermore, the multiphase Mn-Fe-Al-O system exhibits significantly improved reducibility of $Fe_2O_3$ and increased hydrogen production compared to the Fe-Al-O system [60]. Subsequent sections will explore the impact of surface structural and compositional changes in EAFS on its performance characteristics.

### 3.2. Effects of surface modification

The effect of EAFS modification on the reactivity of $Fe_2O_3$/EAFS was further investigated. Given that EAFS has a vitreous structure with a relatively hard surface, it was ground, and its surface was treated with acid and alkali, respectively. As shown in Fig. 2, the surface of $Fe_2O_3$/raw EAFS is rough and irregular, with numerous pores. After grinding, the particles became more regular and uniform. However, following different activation treatments, structural modifications were evident in the $Fe_2O_3$/EAFS samples, including a reduction in pore size and a smoother surface. The specific surface area and pore volume of EAFS after various treatments are presented in Table 3. Neither physical grinding nor acetic acid washing after grinding significantly altered the specific surface area or pore volume of the samples. Physical grinding primarily breaks up the adhesion between EAFS particles without affecting the internal pore volume of each particle. After acid etching, SEM analysis revealed the formation of new particle adhesion, resulting in a strip-like structure. However, as shown in Fig. 3d, after NaOH treatment, finer particles were generated on the surface, potentially blocking some of the EAFS pores. This resulted in a reduction of specific surface area and pore volume to half of that observed in the untreated sample.

Corn stalk CLG experiments were conducted at a constant temperature of 800 °C and an $\Omega$ of 0.2. Fig. 4 presents a comparative analysis of the performance of OCs prepared from EAFS, following various surface physical and chemical modifications, in the hydrogen production process. Specifically, Fig 4a compares the hydrogen production performance of $Fe_2O_3$/EAFS after 1 h and 3 h grinding treatments. The results show that the $Fe_2O_3$/EAFS sample ground for 1 h produced a maximum hydrogen flow rate of 5.5 mL/min, while the sample subjected to 3 h of grinding achieved a higher hydrogen yield of 8.2 mL/min. However, it is important to note that, despite the improvement with extended grinding, the maximum hydrogen production of both ground samples remained lower than that of the original, unground EAFS.

We further investigated the impact of acid and alkali immersion treatments on the catalytic activity of EAFS in the CLG process, with the relevant results presented in Fig. 4b. The performance of acid immersion treatment proved unsatisfactory; when EAFS was treated with a 1 mol/L HCl solution, the maximum hydrogen production rate achieved in the biomass CLG system using EAFS as the support was only 4.4 mL/min. In contrast, alkali immersion treatment demonstrated a potential to enhance reactivity under optimal conditions. Although treatment with 0.5 mol/L and 1.2 mol/L NaOH solutions did not improve the maximum hydrogen flow rate, which remained at 17.9 mL/min and 12.8 mL/min, respectively, compared to untreated EAFS, a notable improvement was observed with 1 mol/L NaOH treatment. Under identical conditions (800 °C and $\Omega = 0.2$), the biomass CLG system using EAFS as the support achieved a significantly higher maximum hydrogen flow rate of 35.3 mL/min.

**Table 3**
BET surface area and Pore volume of EAFS with different activation load on OC.

| | BET surface area ($m^2$/g) | Pore volume($cm^3$/g) |
|---|---|---|
| Raw EAFS | 5.047 | 0.012 |
| 3 h EAFS | 5.285 | 0.013 |
| 1 mol/L HAC EAFS | 5.157 | 0.012 |
| 1 mol/L NaOH EAFS | 2.857 | 0.006 |

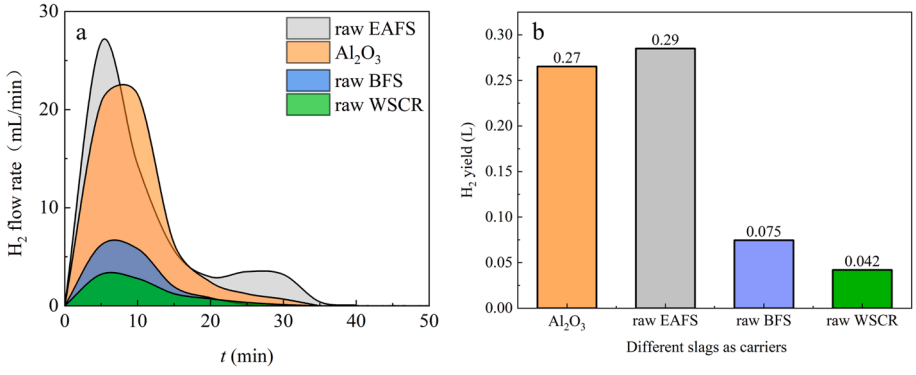


**Fig. 2.** Effect of different slags as carriers on $H_2$ yield during CLG.

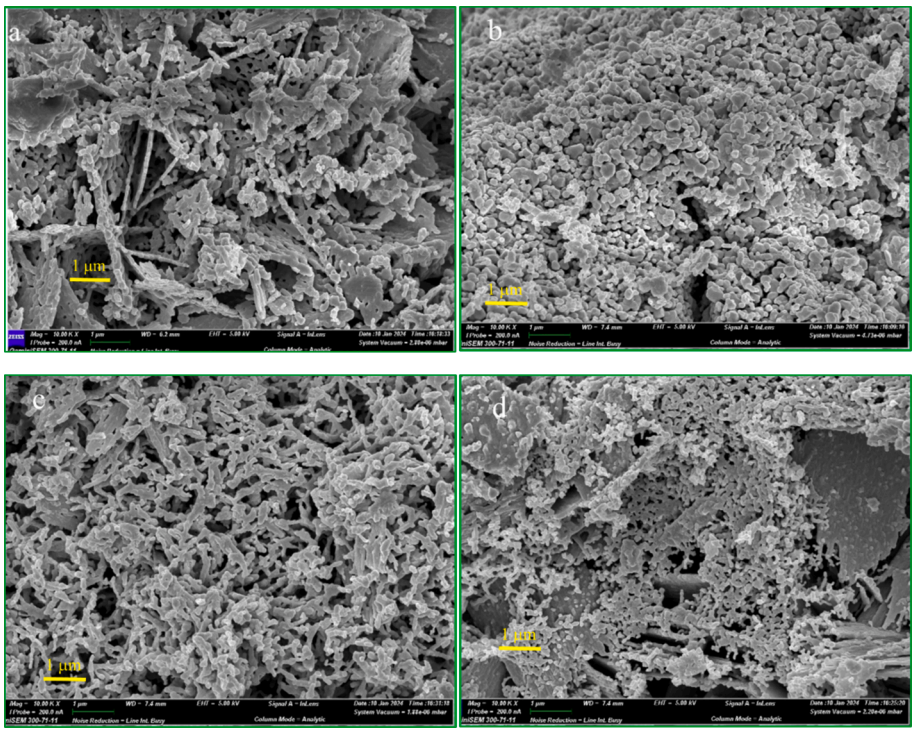


**Fig. 3.** The SEM images for a) the $Fe_2O_3$/raw EAFS, b) $Fe_2O_3$/EAFS with 3 h milling, c) $Fe_2O_3$/EAFS with 1 mol/L HAC acid leaching, and d) $Fe_2O_3$/EAFS with 1 mol/L NaOH alkaline leaching.

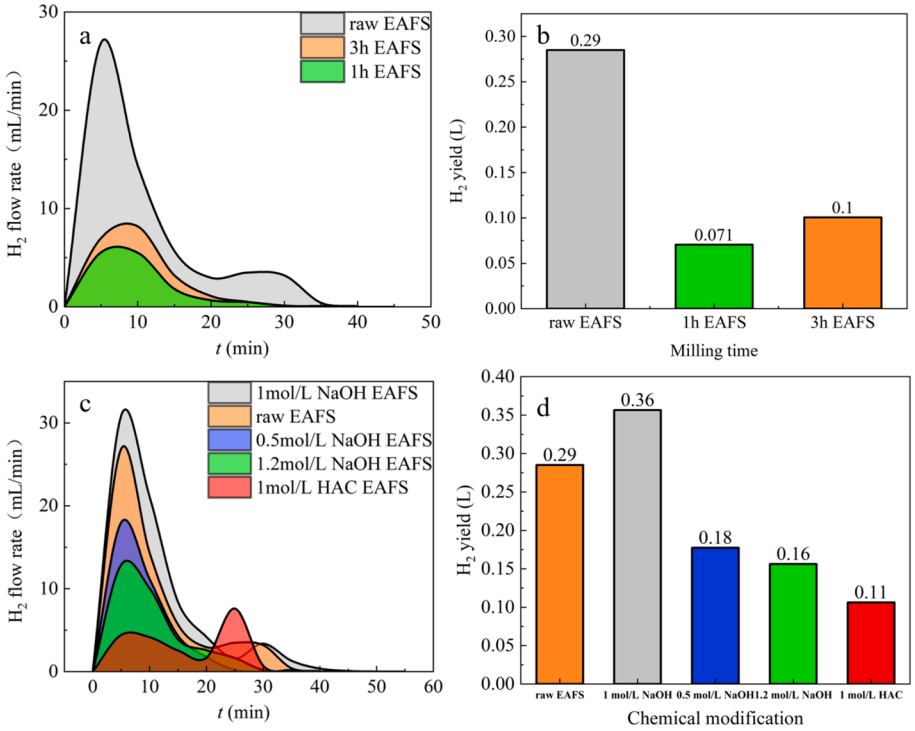


**Fig. 4.** $H_2$ Flow rate of corn stalk CLG process under $T = 800$ °C, $\Omega = 0.2$ using Surface modified $Fe_2O_3$/EAFS: a) Physical modification and b) Chemical modification.

### *3.3. The effects of Ω on hydrogen production in CLG using the NaOH-modified $Fe_2O_3$/EAFS*

A systematic investigation was conducted to evaluate the hydrogen production performance of corn stalk CLG using $Fe_2O_3$/EAFS composite material modified by NaOH, under varying gas flow rates ($\Omega$). The experiments were performed at a constant temperature of 800 °C, with three different $\Omega$ values (0.1, 0.2, and 0.3). The results, presented in Fig. 5, clearly demonstrate that hydrogen production is most pronounced at a gas flow rate of 0.2. At this rate, the maximum hydrogen flow reaches a peak of 35.3 mL/min, which surpasses the hydrogen production observed at the other two flow rates. These findings suggest

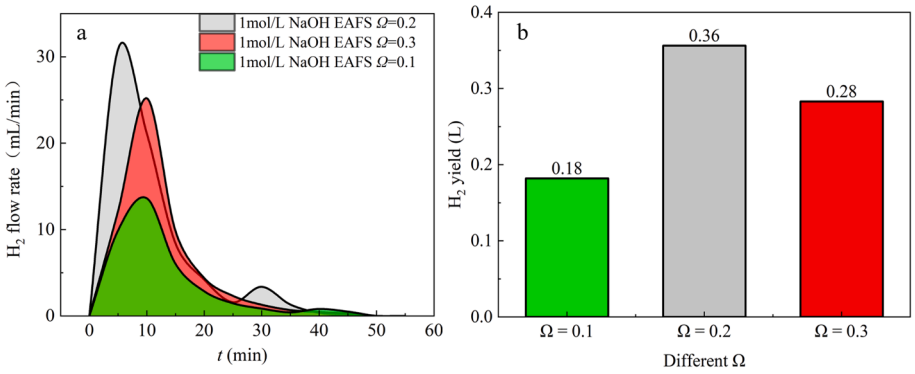


**Fig. 5.** $H_2$ Flow rate of corn stalk CLG process using NaOH-modified $Fe_2O_3$/EAFS under different $\Omega$.

that, under these specific conditions, the interaction between the OC and biomass is more efficient, leading to enhanced hydrogen generation efficiency.

Further analysis indicates that at a gas flow rate of 0.2, the highest cumulative hydrogen production of 332.9 mL was achieved over the course of the experimental process. This result demonstrates that optimizing the gas flow rate to 0.2 not only enhances the hydrogen production rate per unit time but also increases the total hydrogen yield throughout the CLG process. These findings underscore the critical role of gas flow rate in improving the efficiency of hydrogen production in CLG. In conclusion, our study on NaOH-modified $Fe_2O_3$/EAFS OCs confirms its superior catalytic activity at an optimized gas flow rate ($\Omega$ = 0.2), providing valuable insights for the design and optimization of biomass CLG for hydrogen production. Moreover, this suggests that future research could focus on exploring more efficient and stable pathways for biomass gasification by further refining OC modification techniques and optimizing reaction conditions.

### 3.4. The effects of temperature on hydrogen production in CLG using the NaOH-modified $Fe_2O_3$/EAFS

A comprehensive investigation was carried out using NaOH-modified $Fe_2O_3$/EAFS at $\Omega$ = 0.2 to evaluate the efficiency of corn stalk CLG across different temperatures. The hydrogen production results at varying temperatures are depicted in Fig. 6. At temperature of 700 °C, the catalytic activity of the OC was likely insufficient to effectively drive the biomass gasification reaction, resulting in a low hydrogen production rate and indicating inefficient gasification at this temperature. However, when the temperature was increased to 750 °C, the hydrogen yield reached its peak at 559.4 mL. This result suggests that 750 °C may represent the optimal temperature, where the catalyst exhibits moderate redox activity, facilitating efficient biomass gasification without excessive oxidation that would otherwise convert hydrogen into water vapor. Conversely, at 800 °C, an unexpected decline in hydrogen production was observed, despite the anticipated increase in reaction rates at higher temperatures. At this point, the heightened oxidation activity of the OC surpassed the ideal reduction–oxidation equilibrium, leading to substantial recombination of hydrogen and oxygen to form water [61]. Furthermore, intensified oxidation of carbon-based compounds, including $CH_4$ and CO, contributed to a reduction in net hydrogen yield, thereby decreasing the overall energy conversion efficiency of the system. Based on the experimental data, 750 °C was determined to be the optimal temperature for maximizing hydrogen production under the conditions tested.

### 3.5. Analysis of carbon conversion rate

Using NaOH-modified $Fe_2O_3$/EAFS as the OC, corn stalk CLG experiments were conducted under the optimized conditions of 750°C and $\Omega$ of 0.2. Accordingly, the total carbon-containing gas volume ($Q_C$) is the sum of $Q_{CH_4}$, $Q_{CO}$ and $Q_{CO_2}$, is calculated as

$$Q_C = Q_{CH_4} + Q_{CO} + Q_{CO_2} \tag{12}$$

The molar amount of carbon conversion ($n_C$) in the corn stalk CLG process could be expressed as

$$n_C = \frac{Q_C}{24.45} \tag{13}$$

The carbon conversion rate ($r_C$)was calculated as

$$r_c = \frac{dn_c}{m_{oc}dt} \tag{14}$$

where $m_{oc}$ is the mass of the used OC ($Fe_2O_3$/EAFS). Fig. 7 illustrates the gradual increase in $r_c$ during the pyrolysis of corn stalk. In the initial stage of pyrolysis, a rapid release of volatile compounds from the biomass occurs, playing a critical role in increasing $r_c$. This effect can be

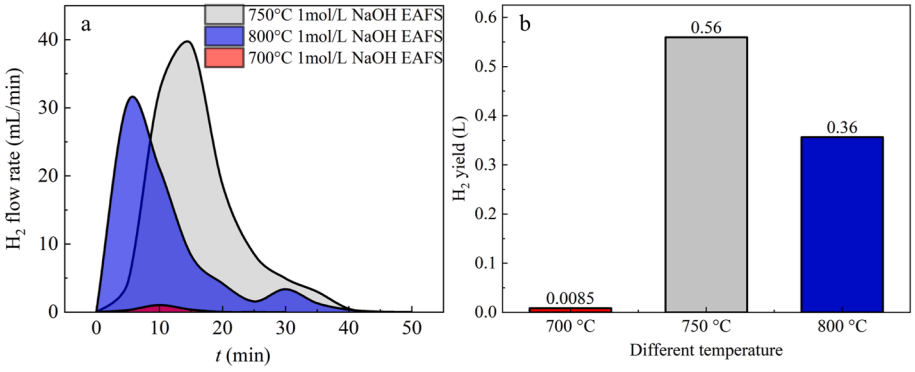


**Fig. 6.** $H_2$ Flow rate of corn stalk CLG process using NaOH-modified $Fe_2O_3$/EAFS under different temperature.

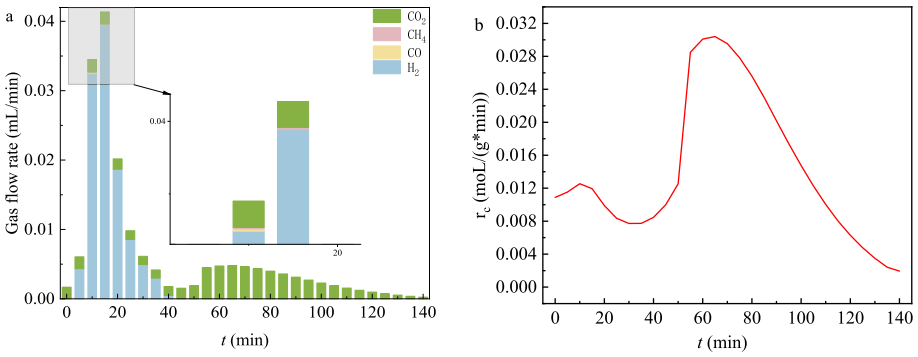


**Fig. 7.** Flow rate distribution of carbon containing gas products a) and carbon conversion rate $r_c$ (mol/(g.min)) b).

attributed to the breakdown of the corn stalk lignocellulosic structure under elevated temperatures, which releases significant quantities of volatile organic compounds (VOCs), including water vapor, light hydrocarbons, and other gases [62]. The release of these volatiles creates additional surface area for the remaining solid residue to interact with both heat and OC (in this case, NaOH-modified $Fe_2O_3$/EAFS), thereby accelerating the overall rate of carbon conversion by promoting further decomposition reactions and accelerating the conversion of carbon into gaseous products. A peak in carbon conversion is observed around 80 min, at which point the maximum carbon conversion rate reaches 0.03 mol/(g·min). At this stage, the system achieves an optimal balance between the supply of reactant biomass and the rate of its conversion. Beyond this point, the rate may decrease, potentially due to factors such as the depletion of readily available biomass components a reduction in the reactivity of residual char, or the deactivation of OC. This experimental result highlights the critical importance of understanding the kinetics and mechanisms underpinning the CLG process. It provides significant insights into how operational parameters such as temperature, $\Omega$, and the type of OC influence the efficiency of biomass conversion into syngas. Future studies should focus on strategies to sustain or enhance peak carbon conversion rates throughout the CLG process, aiming to improve the overall yield and performance in producing hydrogen and other valuable chemicals.

### 3.6. Thermal dynamics analysis

The thermodynamic properties of the system were analysed based on the relevant thermodynamic parameters listed in Table 4.

Thermodynamic analyses were carried out for corn stalk CLG at 750°C, $\Omega = 0.2$ and EAFS subjected to alkaline leaching with 1 mol/L NaOH, as this condition produces the highest gas yield and carbon conversion. For the CLG of $C_4H_6O_3$, $CH_4$ and CO were neglected in the thermodynamic analysis because only 0.00129 L of $CH_4$ and 0.00077 L of CO were obtained during the CLG process, while 0.559 L of $H_2$ and 0.359 L of $CO_2$ were produced. The electron balance analysis showed that the transfer of 0.064 mol of electrons reduces $Fe_2O_3$ to FeO and $Fe_3O_4$. Therefore, the reaction equation can be written as:

$$C_4H_6O_3 + 2Fe_2O_3 + 2H_2O \rightarrow 5H_2 + 3.3CO_2 + 0.6Fe_3O_4 + 2.2FeO + 0.7C$$

Based on the standard molar enthalpy of formation of each reactant and product in the reaction and the reaction enthalpy change formula, the reaction enthalpy of the CLG reaction was calculated to be $\Delta r\, H_{mol} =$ 180.51 kJ/mol.

According to the Kirchhoff equation:

$$\Delta_r H_m^{\ominus}(T) = \Delta_r H_m^{\ominus}(298.15K) + \int_{298.15K}^{T} \Delta_r C_{p,m} dT$$

The enthalpy of reaction of CLG at 1023.15 K was calculated to be $\Delta_r H_m^{\ominus}(1023.15K) = 136.77$ kJ/mol. Therefore, 0.5 g of corn stalk consumed in the CLG reaction contributed to a total reaction enthalpy of 0.67kJ. The reaction is a heat-absorbing process that requires some of the carbon to be burned to provide heat.

**Table 4**
Thermodynamic parameters for various components.

| | $\Delta r\, H_m^{\theta}$ (298.15 K, kJ/mol) | $C_{m,p}$(298.15 K, J/(mol·K)) |
|---|---|---|
| $Fe_2O_3$ | −824.2 | $C_p = 4 \times 10^{-7}T^3$-0.0007 $T^2$ + 0.5649 T-9.9088 |
| FeO | −272 | $C_p = 44.711 + 0.0195$ T-5 $\times 10^{-6}T^2$ |
| $Fe_3O_4$ | −1118.4 | 143.43 |
| $H_2O$ | −241.818 | $C_p = 30 + 10.7 \times 10^{-3}$T-2.022 $\times 10^{-6}T^2$ |
| $H_2$ | 0 | $C_p = 25.399 + 2.0178 \times 10^{-2}$T-3.8549 $\times 10^{-5}T^2 + 3.188 \times 10^{-8}T^3$ |
| C | 0 | $C_p = 17.15 + 4.27 \times 10^{-3}$T-8.79 $\times 10^{-5}T^{-2}$ |
| $CO_2$ | −393.509 | $C_p = 26.75 + 42.258 \times 10^{-3} \times$ T-14.25 $\times 10^{-6} \times T^2$ |
| corn stalk ($C_4H_6O_3$) | −616.49 | 63.43 |

$C_{m,p}$: molar isobaric hot melt.
$\Delta r\, H_m^{\theta}$: standard molar reaction enthalpy.

### 3.7. Characterizations

To further elucidate the composition and structure of surface products treated with NaOH, elemental and X-ray diffraction (XRD) analyses were conducted. Table 5 presents the chemical composition of raw EAFS alongside EAFS subjected to alkaline leaching with NaOH at concentrations of 1 mol/L, 0.5 mol/L, and 1.2 mol/L, as well as EAFS treated with 1 mol/L HAC acid leaching. A comparative analysis of the elemental composition across different surface treatments revealed a marked increase in surface Na content following alkali treatment.

In EAFS, the presence of $Fe_2O_3$, $Al_2O_3$, and $Ca(OH)_2$ can facilitate the formation of $CaFe_2O_4$ at specific temperatures. However, the significance of $CaFe_2O_4$ as OC in this experiment is limited, as it requires temperatures near 1000 °C to exhibit superior oxygen-carrying capacity compared to $Fe_2O_3$ [62]. Notably, when the $Al_2O_3$ mass fraction drops below 1.5 %, $CaFe_2O_4$ decomposes into magnetite and silicate melts. Conversely, when the $Al_2O_3$ mass fraction exceeds 2.5 %, the $CaFe_2O_4$ content increases with rising $Al_2O_3$ levels [63–67]. As shown in Fig. 8, the $Fe_2O_3$/EAFS sample treated with 1 mol/L NaOH, which demonstrated the highest $H_2$ production, exhibits a reduced intensity of $CaFe_2O_4$ diffraction peaks relative to other chemically activated $Fe_2O_3$/EAFS samples.

$NaAlO_2$ is an effective catalyst for gasification, offering greater resistance to deactivation, lower sodium volatility, and higher ash fusion temperatures [57]. The treatment with 1 mol/L NaOH alkaline leaching facilitates the conversion of a significant portion of $Al_2O_3$ into $NaAlO_2$ within the EAFS matrix. However, crystalline $NaAlO_2$ phases are not detected, likely due to the high dispersion of $NaAlO_2$ in an amorphous

**Table 5**
The chemical components of raw EAFS, EAFS with 1 mol/L NaOH alkaline leaching, EAFS with 0.5 mol/L NaOH alkaline leaching, EAFS with 1.2 mol/L NaOH alkaline leaching and EAFS with 1 mol/L HAC acid leaching.

| Chemical components | O | Fe | Ca | Si | Mn | Mg | Al | Na |
|---|---|---|---|---|---|---|---|---|
| EAFS | 33.850 | 26.435 | 19.675 | 6.176 | 5.267 | 4.520 | 1.858 | 0.153 |
| 1 mol/L NaOH EAFS | 32.393 | 21.545 | 17.287 | 5.294 | 4.320 | 1.941 | 1.804 | 13.439 |
| 0.5 mol/L NaOH EAFS | 32.518 | 22.537 | 19.069 | 5.388 | 4.675 | 2.121 | 1.591 | 9.786 |
| 1.2 mol/L NaOH EAFS | 31.780 | 21.687 | 17.192 | 4.553 | 4.521 | 1.702 | 1.703 | 14.899 |
| 1 mol/L HAC EAFS | 34.638 | 25.075 | 19.256 | 7.807 | 5.138 | 3.449 | 1.949 | 0.093 |

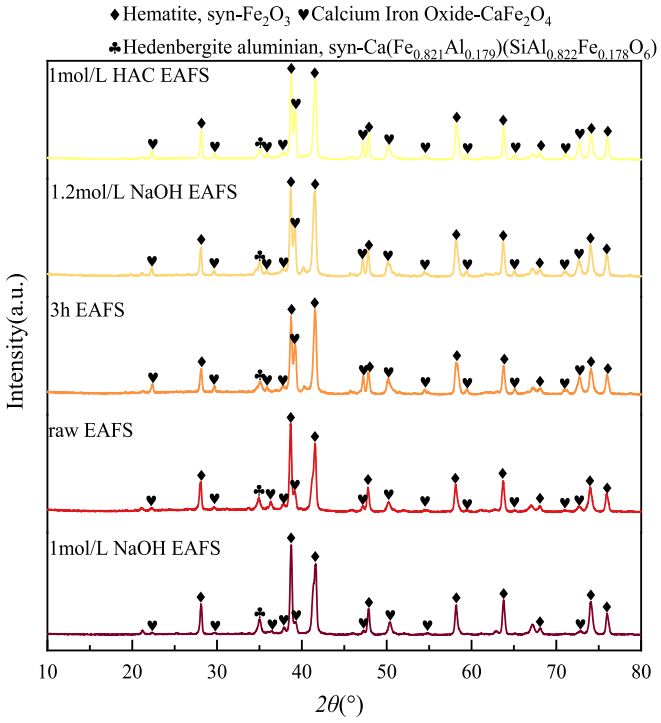


**Fig. 8.** XRD patterns of EAFS with different chemical activation loaded on OC.

state [68].

The treatment of OCs with NaOH introduces Na on their surface, which exhibits fluidity and volatility [69]. This high volatility of Na can generate richer pore structures on the OCs' surface, increasing the number of reactive sites available for gasification reactions [70]. Na can migrate to the interior of carbon grains to form intercalation compounds, disrupting the regular microcrystalline structure of graphitized carbon and activating it into amorphous carbon. Na in $NaAlO_2$ forms the intermediate C-O-Na structure that alters the electron cloud density distribution on the surface of coke. This change reduces the strength of C–C bonds, making them more prone to fracture and forming CO [71–73]. The adjacent carbon atoms become positively charged, facilitating the adsorption of $CO_2$ and $H_2O$ molecules onto these positively charged edge carbon atoms. The presence of $CO_2$ and $H_2O$ enhances the oxidation of carbon atoms, leading to the formation of carbon oxides and accelerating the gasification reaction rate [53,54]. In addition, traditional alkali metal catalysts such as $Na_2CO_3$ have high volatility, rapid loss of catalytic activity, and low ash melting temperature, which can easily lead to reactor corrosion and scaling. In contrast, $NaAlO_2$ has lower alkali volatility and higher ash melting temperature [74], which can alleviate corrosion and scaling problems and contributes to more efficient and sustainable gasification processes than traditional alkali metal catalysts [75,76].

Consequently, optimizing activation methods is crucial for tailoring the composition and properties of $Fe_2O_3$/EAFS to enhance hydrogen production efficiency. In the future, we plan to develop an OC with a core–shell structure to further reduce alkali metal volatilization losses, while suppressing the migration of Fe ions from the interior to the surface, avoiding the enrichment of metal Fe on the surface, and increasing the sintering resistance of OC. The shell can not only improve the stability of OC structure, but also promote the oxygen lattice transfer rate [77].

## 4. Conclusions

$Fe_2O_3$/EAFS emerges as a promising OC for biomass CLG in hydrogen production, surpassing BFS in both reactivity and suitability. Surface modification techniques, notably treatment with a 1 mol/L sodium hydroxide solution, significantly enhance the performance of EAFS in biomass CLG, achieving a remarkable hydrogen production rate of 0.559 L per 0.5 g of corn stalk at $\Omega$ of 0.2 and T of 750 °C. Compared to untreated EAFS, the hydrogen production of EAFS with 1 mol/L NaOH treatment increased by 1.24 times. Thermodynamic and kinetic analyses further demonstrate the potential of chemically activated slag to improve both carbon conversion and hydrogen yield during biomass CLG. Mechanistic insights, obtained through XRD, SEM, and BET analyses, elucidate the activation process, highlighting the critical role of polycrystalline grain boundary effects in enhancing both reactivity and selectivity. These findings underscore the crucial importance of surface modification technologies in optimizing the physicochemical properties of slag, thereby enabling more efficient biomass CLG and addressing pressing challenges in energy conversion and solid waste management. The application of $Fe_2O_3$/EAFS as OC in chemical looping processes holds promise for sustainable development, offering significant energy and environmental benefits through the efficient utilization of resources.

## CRediT authorship contribution statement

**Laixing Luo:** Writing – original draft, Visualization, Investigation, Formal analysis, Data curation. **Zhihang Lai:** Writing – original draft, Visualization, Formal analysis, Data curation. **Xing Zheng:** Visualization, Validation, Data curation. **Zongming Zheng:** Resources, Project administration, Methodology, Investigation, Funding acquisition. **Xianbin Xiao:** Supervision, Project administration, Methodology, Investigation, Funding acquisition. **Wu Qin:** Writing – review & editing, Resources, Project administration, Methodology, Investigation, Funding acquisition, Conceptualization.

## Declaration of competing interest

The authors declare that they have no known competing financial interests or personal relationships that could have appeared to influence the work reported in this paper.

## Acknowledgments

The authors wish to thank the National Key Research and Development Program of China (2021YFE0194500) and the National Natural Science Foundation of China (32171915).

## Data availability

Data will be made available on request.

## References


[1] Ishida M, Jin H. A new advanced power-generation system using chemical-looping combustion. Energy 1994;19(4):415–22.
[2] Wang JX, Sun YH. Review of Chemical-looping combustion technology research. J North China Electric Power Univ (Natural Science Edition) 2019;46(5):100–10.
[3] Jin HG, Hong H, Wang BQ, Han W, Lin RM. Principles of integrated gradient utilization of chemical and physical energy. Sci China Ser. E Eng Mater Sci 2005;35 (3):299–313.
[4] Wang BW, Zhao HB, Zheng Y, Liu ZH, Zheng CG. Research progress in chemical looping combustion of coal. Dongli Gongcheng Xuebao/Journal of Chinese Society of Power Engineering 2011;31(7):544–50.
[5] Bhavsar S, Najera M, Veser G. Chemical looping dry reforming as novel, intensified process for $CO_2$ activation. Chem Eng Technol 2012;35(7):1281–90.
[6] Fan LS, Shwetha R, Li FX. Utilization of chemical looping strategy in coal gasification processes. Particuology 2008.
[7] Shen L, Wu J, Gao Z, Xiao J. Characterization of chemical looping combustion of coal in a 1 kW th reactor with a nickel-based oxygen carrier. Combust Flame 2010; 157(5):934–42.
[8] Udomsirichakorn J, Basu P, Abdul Salam P, Acharya B. CaO-based chemical looping gasification of biomass for hydrogen-enriched gas production with in situ $CO_2$ capture and tar reduction. Fuel Process Tech 2014;127:7–12.
[9] Wei GQ, He F, Zhao ZL, Zhao WN, Huang Z, Zheng AQ, et al. Chemical looping gasification of biomass based on the oxygen carrier derived from the layered double hydroxide(LDH) precursor. J Fuel Chem Technol 2016;44(3):8.
[10] Niu X. Chemical looping combustion of sewage sludge and Nitrogen-Phosphorus transformation. Southeast University; 2017.
[11] Tian X, Niu P, Ma Y, Zhao H. Chemical-looping gasification of biomass: Part II. Tar yields and distributions. Biomass Bioenerg 2018;108:178–89.
[12] Deng ZB, Huang Z, Zheng AQ, He F, Wei GQ, Zhao ZL, et al. Thermodynamic analysis and experimental study of nitrongen migration during the sludge chemical looping gasification using iron based oxygen carriers. Adv New Renew Energy 2019;7(3):199–206.
[13] Tang GY, Gu J, Yang Q, Huang Z, Yuam HR, Chen Y. Research progress in chemical looping gasification technology of organic solid waste. Acta Petrolei Sinica (Petroleum Processing Section) 2021;37(3):19.
[14] Cabello A, Dueso C, Garcia-Labiano F, Gayan P, Abad A, Diego LD, et al. Performance of a highly reactive impregnated $Fe_2O_3/Al_2O_3$ oxygen carrier with $CH_4$ and $H_2S$ in a 500 Wth CLC unit. Fuel 2014;121:117–25.
[15] Guo WJ, Ge HJ, Shen LH, Song T, Gu HM, Jiang SX. Experimental study on chemical looping gasfication of biomass with hematite base on 25$kW_{th}$ fluidized beds. J Therm Sci Tech 2017;16(1):9.
[16] Huang Z, Liu S, Li DB, Zhan ZG, He F, Li HB. Thermodynamic simulation of chemical looping gasification of biomass based on $Fe_2O_3$ oxygen carriers. Acta Energiae Solaris Sinica 2017;38(5):10.
[17] Ismail M, Liu W, Scott SA. The performance of $Fe_2O_3$-CaO Oxygen Carriers and the Interaction of Iron Oxides with CaO during Chemical Looping Combustion and $H_2$ production. Energy Procedia 2014;63:87–97.
[18] Hua X, Wang W, Wang F. Performance and kinetics of iron-based oxygen carriers reduced by carbon monoxide for chemical looping combustion. Front Env Sci Eng 2015;9:1130–8.
[19] Qi B, Xia Z, Huang GY, Wang W. Study of chemical looping co-gasification(CLCG) of coal and rice husk with an iron-based oxygen carrier via solid–solid reactions. J Energy Inst 2017;92:382–90.
[20] Schanz E, Pröll T, Hofbauer H. Performance of an iron based oxygen carrier in a 120 kWth chemical looping combustion pilot plant. Fuel 2018;217:561–9.
[21] Wang BW, Li HY, Ding N, Shen QW, Zhao HB, Zheng CG. Chemical looping combustion characteristics of coal with $Fe_2O_3$ oxygen carrier. J Therm Anal Calorimetry 2018;132:17–27.
[22] Wang BW, Zhao HB, Zheng Y, Liu ZH, Zheng CG, Yan R. Effect of inert support $Al_2O_3$ on the chemical looping combustion of coal with $Fe_2O_3$ and CuO-based oxygen carrier. Proc CSEE 2011;31:53–61.
[23] Wang XY, Xiao XB, Zheng ZM, Qin W. Preparation and chemical looping reaction activity of iron-based oxygen carriers. Guangdong Chem Industry 2019;46(21):4.
[24] Wei ZH, Liu DC, Jin JJ, Li WY. Research progress on Fe-based oxygen carrier in chemical looping combustion. Clean Coal Technology 2019;25(3):9.
[25] Abuelgasim S, Wang WJ, Li TL, Cao YG, Abdalazeez A. Optimizing oxygen uncoupling performance and stability of novel $MgO/TiO_2$ supported CuO oxygen carrier: Effect of impregnation steps and $ZrO_2$ addition. Sep Purif Technol 2023; 326:124827.
[26] Jw Hu, Galvita VV, Poelman H, Detavernier C, Marin GB. A core-shell structured $Fe_2O_3/ZrO_2$@$ZrO_2$ nanomaterial with enhanced redox activity and stability for $CO_2$ conversion. J $CO_2$ Util 2017;17:20–31.
[27] Zhou YM, Dai RD. Return of electric furnace slag to blast furnace smelting. Iron Steel 1981;2:74–5.
[28] Shi ZY, Zhao CM. Application of electric furnace white slag powder in desulphurisation of molten iron. Ironmaking 1985;63:33–6.
[29] Qin JY. Production of steel slag white cement and its products by using reduced slag from electric furnace. Environmen tal Protection and Technology 1990;4: 25–9.
[30] Zheng H, Jia CH, Wang JG, Ma ZC, Wang WH, Dong GW. Research on recycling process of reduction slag in electric furnace. Heilongjiang Metallurgy 2003;1:5–6.
[31] Chen SJ, Gao HL. Comprehensive utilization of steel -making slag and its prospects. Southern Metals 2004;41:1–4.
[32] Geng Z. Status of coprehensive utilization of steel slag at baosteel. Baosteel Technology 2006;1:25–9.
[33] Cheng X. Study on preparation and properties of ZTA ceramics using blast furnace slag as sintering aids. Zhengzhou University; 2017.
[34] Ren YS. Fundamental technology study on agriculture utilization of solid aste from iron and steel industry. Tianjin University; 2007.
[35] Wei W. Experimental study on preparation of ceramic by titania-bearing blast slag and its exploratory research on antibacterial performance. Northeastern University; 2010.
[36] Wang Z, Liu J, Chen L, Huang G. Adsorption capability of blast furnace slag to $Cd^{2+}$. Environ Prot Chem Indus 2015;35(2):5.
[37] Zhong S. Performance experimental and application study on high-titanium blast furnace slag no-sand concrete. Xihua University 2017.
[38] Liu X, Zhang C, Xu YJ, Guo P. Large-scale direct shear test of shear strength characteristics of blast furnace slag modified mixture. Soil Eng Foundation 2018;32 (6):4.
[39] Zhou CL. Experimental study on high-titanium blast furnace slag heat-resistant concrete. Bull Chin Ceramic Soc 2018;37(10):88–92.
[40] Yang ZY, Yao ZY. Development of fast gunning mass for vanadium recovering converter and its application. Sichuan Metall 2019;41(4):4.
[41] Duan WJ, Gao YK. A review on effects of composition on the preparation of glass ceramics from blast furnace slag. J Mater Metall 2020;19(3):8.
[42] Liang ZY, Zhang H, Ma ML, Ban SP, Yang H. Effect of firing process system on performance of foamed ceramic prepared by titanium-bearing blast furnace slag. Bull Chin Ceramic Soc 2020;39(5):6.
[43] Lu HX, Gao K, Li ML, Wang HL. Preparation of ZTA/TiC composite ceramics using blast furnace slag as sintering aid. J Zhengzhou Univ (Engineering Science) 2020; 41(5):7.
[44] Yang HY, Guo HL. The progress in preparation of glass-ceramics from industrial solid wastes. Sci Technol Information 2020;18(33):53–5.
[45] Zhou XZ, Ju DC, Tian S, Zhang LR, Yang ZB, Zhou L. Study on adsorption performance of modified blast furnace slag onto $Ce^{3+}$. New Chem Mater 2020;48 (5):5.
[46] Wei NN. Development of glass ceramics for architectural decoration during the 13th five-year plan. Glass 2021;48(4):5.
[47] Gómez-Casero MA, Bueno-Rodríguez S, Castro E, Eliche QD. Alkaline activated cements obtained from ferrous and non-ferrous slags. Electric arc furnace slag, ladle furnace slag, copper slag and silico-manganese slag. Cement Concrete Comp 2024;147:105427.
[48] Wei DX, Xu AJ, He DF, Tian NY, Yang Q. Beneficial reuse of EAF slag and its leaching behavior of Cr. Iron Steel 2012;47(10):5.
[49] Hildor F, Leion H, Linderholm CJ, Mattisson T. Steel converter slag as an oxygen carrier for chemical-looping gasification. Fuel Process Technol 2020;210:106576.
[50] Zhang ZY, Wang XT, Zhang LL, Zhou HT, Ju R, Rao PJ, Guo XY, Han YQ, Chen HW. Characteristics of steel slag as an oxygen carrier for chemical looping gasification of sewage sludge. 2022; 247: 123534.
[51] Dilmaç ÖF, Dilmaç N, Doruk ET. Performance of electric arc furnace slag as oxygen carrier in chemical looping combustion process. Fuel 2020;265:117014.
[52] Di ZC, Cao Y, Yang FL, Cheng FQ, Zhang K. Studies on steel slag as an oxygen carrier for chemical looping combustion. Fuel 2018;226:618–26.
[53] Veraa MJ, Bell AT. Effect of alkali metal catalysts on gasification of coal char. Fuel 1978;57:194–200.
[54] Hamilton RT, Sams DA, Shadman F. Variation of rate during potassium catalysed $CO_2$ gasification of coal char. Fuel 1984;63:1008–12.
[55] Li ZQ, Li Q, Huang W, Ding L, Qiu ZG. Direct synthesis of $C_2$-oxygenates from $CH_4$ and $CO_2$ over acid-modified $CoPd/TiO_2$ catalyst. Chem Industry Eng Progr 2020; 39:1035–42.
[56] Qin W, Luo L, Chen S, Iqbal T, Dong C. Efficient strategy of utilizing alkaline liquid waste boosting biomass chemical looping gasification to produce hydrogen. Fuel Process Tech 2021;217:106818.
[57] Mei Y, Wang Z, Fang Y, Huang J, Li W, Guo S, et al. $CO_2$ catalytic gasification with $NaAlO_2$ addition for its low-volatility and tolerant to deactivate. Fuel 2019;242: 160–6.
[58] Son SR, Kim SD. Chemical-looping combustion with NiO and $Fe_2O_3$ in a thermobalance and circulating fluidized bed reactor with double loops. Ind Eng Chem Res 2006;45(8):2689–96.
[59] Hu J, Li H, Chen S, Xiang W. Enhanced $Fe_2O_3/Al_2O_3$ oxygen carriers for chemical looping steam reforming of methane with different Mg ratios. Ind Eng Chem Res 2022;61:1022–31.
[60] Zeng D, Cui D, Qiu Y, Li M, Ma L, Zhang S, et al. Mn-Fe-Al-O mixed spinel oxides as oxygen carrier for chemical looping hydrogen production with $CO_2$ capture. Fuel 2020;274:117854.
[61] Franco C, Pinto F, Gulyurtlu I, Cabrita I. The study of reactions influencing the biomass steam gasification process. Fuel 2003;82(7):835–42.
[62] Li G, Lv X, Ding C, Zhou X, Zhong D, Qiu G. Non-isothermal carbothermic reduction kinetics of calcium ferrite and hematite as oxygen carriers for chemical looping gasification applications. Appl Energ 2020;262:114604.
[63] Yan LG, Wang YF, Cui LM, Hu CQ. Effect of $Al_2O_3$ content on formation of sintered calcium ferrites under quasi-chmical equilibrium. Foundry Technol 2017;38(4):4.
[64] Wang SC, Hu CQ, Jia JT, Xu WZ, Yan LF. Effects of $SiO_2$ content on the formation of Mg-rich silico-ferrite of calcium and aluminum. Sintering Pelletizing 2018;43(6): 34–7.

[65] Bai K, Shen J, Zhu Z, Zuo H, Pan Y, Wang J, et al. Effect of $Al_2O_3$ on the formation of calcium ferrite in the solid state. Metals 2019;9:681.
[66] Guo H, Guo XM. Effect of alumina on liquid phase formation in sintering process of iron ore fines. Steel Res Int 2019;90(8):1900138.
[67] Xin RF, Guo XM. Effect of $SiO_2$ on crystallization of calcium ferrites in $Fe_2O_3$–CaO–$SiO_2$–$Al_2O_3$ system in cooling process. Metall Mater Trans B 2022;53(3):1904–19.
[68] Zhang Y, Niu S, Lu C, Gong Z, Hu X. Catalytic performance of $NaAlO_2$/γ-$Al_2O_3$ as heterogeneous nanocatalyst for biodiesel production: Optimization using response surface methodology. Energ Convers Manage 2020;203:112263.
[69] Xu B, Cao Q, Kuang D, Gasem KAM, Adidharma H, Ding D. Kinetics and mechanism of $CO_2$ gasification of coal catalyzed by $Na_2CO_3$, $FeCO_3$ and $Na_2CO_3$–$FeCO_3$. J Energy Inst 2020;93(3):922–33.
[70] Wang Y, Wang Z, Huang J, Fang Y. Catalytic gasification activity of $Na_2CO_3$ and comparison with $K_2CO_3$ for a high-aluminum coal char. Energ Fuel 2015;29(11):6988–98.
[71] Malekshahian M, Hill JM. Potassium catalyzed $CO_2$ gasification of petroleum coke at elevated pressures. Fuel Process Technol 2013;113:34–40.
[72] Wang Q, Wang E, Li K, Husnain N, Li D. Synergistic effects and kinetics analysis of biochar with semi-coke during $CO_2$ co-gasification. Energy (Oxford) 2020;191:116528.
[73] González JD, Mondragón F, Espinal JF. Effect of calcium on gasification of carbonaceous materials with $CO_2$: A DFT study. Fuel 2013;114:199–205.
[74] Li T, Zhang L, Dong L, Wang S, Song Y, Wu L. Effects of char chemical structure and AAEM retention in char during the gasification at 900℃ on the changes in low-temperature char-$O_2$ reactivity for Collie sub-bituminous coal. Fuel 2017;195:253–9.
[75] Guo S, Jiang Y, Liu T, Zhao J, Huang J, Fang Y. Investigations on interactions between sodium species and coal char by thermogravimetric analysis. Fuel 2018;214:561–8.
[76] Yang HP, Song H, Zhao C, Hu JH, Li SQ, Chen HP. Catalytic gasification reactivity and mechanism of petroleum coke at high temperature. Fuel 2021;293:120469.
[77] Ma SW, Chen SY, Zhu M, Zhao ZH, Hu J, Wu MD, et al. Enhanced sintering resistance of $Fe_2O_3$/$CeO_2$ oxygen carrier for chemical looping hydrogen generation using core-shell structure. Int J Hydrogen Energ 2019;44(13):6491–504.